USC UNIVERSIDADE DE SANTIAGO DE COMPOSTELA
CAMPUS VIDA CAMPUS DE EXCELENCIA INTERNACIONAL
CiTIUS Centro Singular de Investigación en Tecnoloxías da Información

# A review on CMOS photodiodes modeling, the role of the lateral photoresponse

Beatriz Blanco-Filgueira, Paula López Martínez, and Juan Bautista Roldán Aranda

**Version:** accepted article

## How to cite:

Beatriz Blanco-Filgueira, Paula López Martínez, and Juan Bautista Roldán Aranda (2016) A review on CMOS photodiodes modeling, the role of the lateral photoresponse. IEEE TRANSACTIONS ON ELECTRON DEVICES, 63(1), 16-25.

Doi: 10.1109/TED.2015.2446204

## Copyright information:

© 2016 IEEE. Personal use of this material is permitted. Permission from IEEE must be obtained for all other uses, in any current or future media, including reprinting/republishing this material for advertising or promotional purposes, creating new collective works, for resale or redistribution to servers or lists, or reuse of any copyrighted component of this work in other works.

# A review on CMOS photodiodes modeling, the role of the lateral photoresponse

Beatriz Blanco-Filgueira, Paula López Martínez, Juan Bautista Roldán Aranda,

*Abstract*—**CMOS photodiodes are the primary photosensing devices used in nowadays solid-state image sensors. A review of significative CMOS photodiodes models that can be found in the literature of the last years is presented here. We have focused on photodiodes current models in one, two and three dimensions, and we have paid special attention to lateral current components. Lateral collection, particularly for small photodiodes fabricated in deep submicron technologies, has been shown to be of utmost importance. Finally, several models to account for crosstalk effects are also described.**

*Index Terms*—**Photodiodes, crosstalk, modeling, simulation**

## I. Introduction

THe principle of operation of a photodiode is based on the charge collection through the so-called active area, which is directly exposed to light. However, photocarriers which are generated in the substrate within the device can be also successfully diffused to the junction. The depletion region of the junction is defined by its side-walls and bottom areas, which are responsible for the lateral and bottom collections, respectively. In particular, the collection through the bottom of the depletion region due to photocarriers generated deep in the substrate can be significant for large photodiodes, whereas lateral collection can be somewhat neglected in this case. This latter term acquires special relevance in small photodiodes, particularly in deep submicron technologies.

Compact and accurate physical models of photodiodes are essential for the development of future integrated circuits based on CMOS image sensors. The active area contribution to the total current has to be complemented in current technologies with the lateral photocurrent component. Process engineers can benefit from them in designing new devices since physical parameters and geometrical information affect the electrical device performance.

Good models can help to assess the impact of technology scaling and the optimum photodiode size for enhanced sensitivity. In addition, models represent the link to the broad terrain of circuit design. This is achieved by means of the implementation of device models within circuit simulators. The accuracy of circuit design lies upon reliable models and these models can be decisive for the choice of a particular technology to build an integrated circuit.

In this context we present this review of photodiodes current models. We have paid special attention to the lateral photoresponse taking into consideration that it is essential in nowadays highly scaled CMOS photodiodes. Our revision starts from the very first approaches in the 70s. The historical development is outlined in Section II. Next, we will perform an extended explanation of the different types of models that can be found in the literature in Sections III and IV of our manuscript. We do not pretend to include all of them; nevertheless, we will comment on a representative set, trying to classify them accounting for their semyanalytical, analytical or numerical nature as well as for whether they consider a 1D, 2D or 3D approach, including some of the models we have recently developed.

Electrical crosstalk will be defined within this manuscript as the unwanted component of the photodiode output signal which is originated from photocarriers generated by illumination of other photodiodes in the vicinity and is not to be confused with lateral collection. Within this framework we review in Section V the main results published so far regarding the analytical modeling of crosstalk in CMOS image sensors highlighting the importance of the pixel size.

## II. Historical development of CMOS photodiode modeling

Although the first solid-state image sensors were already proposed in the 1960s decade, [1]–[8], the effect of Fixed-Pattern Noise (FPN), firstly explored in the 1970s, was deemed a major drawback of CMOS image sensors, [9]. For this reason, Charge Coupled Devices (CCD), introduced in 1970 and more immune to FPN, [10], became the reference for solid state image sensor technologies, [11], [12]. The development of CMOS Active Pixel Sensor (APS) (introduced in 1968, [6]) started at the beginning of the nineties, but it was not until the incorporation of integrated microlenses in sub-micron CMOS technologies and the development of new techniques for the reduction of the thickness of the interconnect section that APS became a real competitor to CCDs, [13]. The semiconductor industry unstoppable technology scaling race helped for this change to occur. In particular, as published in [14], an ADC was integrated in each pixel in the Digital Pixel Sensor (DPS). New applications in the broad terrain of solid state image sensors showed up due to the high speed readout that came afterwards, [15].

This work has been partially supported by the Spanish Government under projects TEC2009-12686 and TEC2012-38921-C02-02 (European Region Development Fund, ERDF/FEDER), by the Xunta de Galicia under projects EM2013/038 and GPC2013/040 (ERDF/FEDER), by the Junta de Andalucía under project FQM.1861 and by AE CITIUS under the project CN2012/151 of the Xunta de Galicia (ERDF/FEDER).

B. Blanco-Filgueira and P. López are with the Centro de Investigación en Tecnologías de la Información (CITIUS), University of Santiago de Compostela, Santiago de Compostela 15782, Spain.

J. B. Roldán is with the Department of Electronics and Computer Technology, University of Granada, Granada 18071, Spain.

Continuous CMOS fabrication technological advances, as well as the use of transistor-sharing approaches, [16], made possible the reduction of the pixel size beyond the optical diffraction limit. The effect of the pixel size reduction on the performance characteristics of CMOS imagers has been analysed by different authors, [17]–[22]. These studies highlight the need of a reliable tool to predict the amount of photocurrent that will be generated for a given incident light, photodiode characteristics and fabrication process technology. This tool is a compact model, essential in the toolbox of process engineers and circuit designers; it is well known that technology improvements in the integrated circuit arena go hand by hand with the corresponding modeling improvements.

Photogenerated current physical models in CMOS photodiodes dating back to the 70s can be found in the literature, [23], [24]. In the first of these models, [23], an analytical 1D expression as well as 2D numerical approach are derived, representing, to the best of our knowledge, the first study of the lateral photocurrent on CMOS photodiodes. The latter model, [24], published just one year later, studies the same effect from a 2D perspective, albeit for large photodiodes with particular symmetries. Later, 2D and 3D studies were presented in 1983 and 1987 respectively, but compact solutions could only be derived for particular cases, [25], [26]. The continuous scaling of pixel sizes on advanced CMOS technologies has triggered the publication of multiple photodiode models in the literature in the last years, [27]–[47], which highlights the importance of being able to predict the photocurrent generated by a given structure for certain illumination conditions.

In the next sections we will try to review the main photocurrent models present in the literature in an organized manner, taking into account the different devices targeted, number of dimensions considered and mathematical approaches. We do not pretend to include all of them but we will comment on a representative set. Most of them correspond to either p-n$^+$ or p-n$_{\text{well}}$ uniformly illuminated devices such as the ones shown in Fig. 1(a) and (b) respectively, where the main geometrical parameters are shown. The n$^+$ diffusion, the n-well diffusion and the whole device are $x_{\text{ph}}$, $x_{\text{well}}$ and $x_\ell$ wide, respectively, and $x_s$ represents the distance between the edge of the depletion region and the lateral limit of the photodiode. The wafer thickness is $y_{\text{w}}$ and $y_{ph}$ and $y_{\text{j}}$ stand for the n$^+$ over n-well penetration and the junction depth, respectively. In reverse-bias operation three main regions are distinguished: two quasi-neutral regions and the depletion region with thickness $W$ (in y-direction) and $W_\ell$ (in x-direction).

## III. First approaches: semianalytical models

Even though a three-dimensional treatment is regarded the best way to proceed, for the sake of simplicity, a semianalytical approximation to experimental data can be very useful for certain applications. These kind of strategies are of most interest in the compact modeling and circuit simulation arena.

In 2006, a novel structure which showed the benefits of the peripheral utilization effect was presented, [48]. It consisted of a photodiode where the total peripheral length was increased by opening circular holes on its diffusion area. A test chip

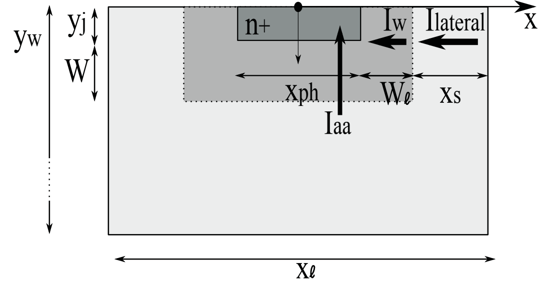


(a) Cross section of a p-n$^+$ photodiode.

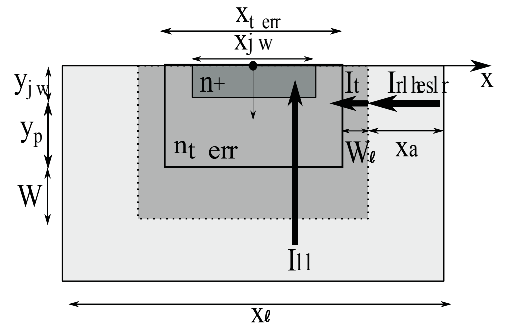


(b) Cross section of a p-nwell photodiode.

Fig. 1. Cross section of a p-n$^+$ (top) and a p-nwell (bottom) photodiode showing the main geometrical parameters.

with several APS cells with 7, 11, 14 and 17 openings as well as a reference pixel was designed, fabricated and tested in a 0.5 $\mu$m CMOS process, demonstrating an improvement of the spectral response of the pixel. This study was extended in [49], showing that for the photodiode with 17 circular openings under a 390 nm light source, the quantum efficiency and the pixel full-well capacity improved 12 % and 22 %, respectively, at the expense of doubling dark current compared with the reference pixel. Models for characteristic magnitudes can be found in [49].

Although the work by S. U. Ay demonstrated the importance of peripheral collection, no efforts were made on mathematically quantifying its effect on the pixel photocurrent. The first semianalytical model of a CMOS pixel photoresponse including the peripheral collection was presented in [27], where an expression for the CMOS APS photosignal in terms of the geometrical shape and process data was derived. For a device such as the one in Fig. 1(a), this expression results in,

$$\frac{V_{\text{out}}(\lambda)}{N_{\text{ph}}} = \frac{k_1\, x_{\text{ph}}^2 + k_2\, 4x_{\text{ph}}(y_j + W)\frac{x_\ell^2 - x_{\text{ph}}^2}{x_\ell^2}\left(1 - \frac{x_\ell - x_{\text{ph}}}{2L_n}\right)}{k_3\, x_{\text{ph}}^2 + k_4\, 4x_{\text{ph}}} \tag{1}$$

where $N_{\text{ph}}$ is the number of incoming photons (in a time unit), $k_1$, $k_2$ are wavelength dependent fitting parameters, $k_3$ and $k_4$ describe the bottom and side-wall capacities and $L_n$ is

the electron diffusion length. The model was compared with measurements from a CMOS APS image sensor fabricated in a standard 0.5 $\mu$m CMOS process. The test chip included pixel sets of square, rectangular, circular, and L-shaped active areas of different sizes. The study of their photoresponse for different wavelengths in the visible range showed that longer wavelengths enabled better response. And, more importantly, a trade-off between the active area size and the peripheral collection to enable the maximum photoresponse was found. Later, this model was used to predict the maximum pixel response in scalable CMOS technologies, [28], showing that the scaling influence depends on a large variety of parameters and an analytical expression determining the scaling trends could not be derived. The proposed approximation assumes that the ratio between the unity active area and the unity periphery contributions has a slight upward trend, mostly through the reduction of mobility and lifetime with increasing doping levels, and a shrinkage of the depletion widths. A test array in a 0.35 $\mu$m CMOS process was measured to compare the experimental results and the theoretically predicted response, showing good agreement.

Another study of the peripheral photoresponse and crosstalk by the same authors was presented in [29]. Experimental measurements of several pixel topologies of CMOS APS in a standard 0.35 $\mu$m technology were performed using a submicron scanning system. The data include the pixel response and the crosstalk from each of the neighbours as a function of the photodiode dimension and the wavelength of the incident light. The peripheral photoresponse was also studied by means of numerical device simulations based on the parameters of the technology employed for the chip fabrication. A set of simulations for different values of the wavelength and the distance between the depletion boundary and the illumination point were carried out to study the photocarrier concentration and its two-dimensional distribution. As different wavelength illuminations cause different photocarrier distributions in the semiconductor depth, the original semianalytical model for the photoresponse estimation was enhanced by the separation of the lateral and bottom diffusion contributions. In addition, the improved model was applied to the crosstalk analysis and successfully compared with experimental results. However, no results in smaller technological nodes were reported.

A semianalytical model based on [27]–[29] for the photoresponse estimation of a 3-transistor (3T) APS with p-$n^+$ and p-$n_{\text{well}}$ junction photodiodes in 180 nm and 90 nm technologies was later proposed. The aim of this approach was to take into account the physical phenomena which affect these devices in new technological nodes. Specifically, the model takes into account the differences between the active area and peripheral contributions in terms of the photodiode dimensions. Several functions to model the bottom and the active area contributions were also proposed and compared. The model was tested with fabricated 3T-APS octagonal p-$n^+$ and square p-$n_{\text{well}}$ junctions in UMC 180 nm CIS and 90 nm standard technologies, respectively, showing an accurate agreement with experimental data. The results were reported in [30]–[33].

## IV. Analytical models

There is a large variety of analytical models for photodetectors in the literature which can be classified according to different criteria such us the dimension (1D, 2D or 3D), the features of the modeled devices (vertical, lateral, mesa, finger, backside illuminated, etc.), the sort of junction (p-$n^+$, n-$p^+$, p-$n_{\text{well}}$, $n_{\text{well}}$-$p^+$, p-epi-$n_{\text{well}}$, p-epi-$p_{\text{well}}$-$n^+$, etc.), the application frequency range (gamma ray, X-ray, ultraviolet, visible, infrared, microwave, etc.), and other characteristics. Moreover, boundary conditions and simplifications may vary from one model to another further complicating the classification. For this reason, although a collection of the most representative modeling efforts found in the literature is revised in this section, a direct comparison of their performance is not possible.

Regardless of the approach considered, the steady-state continuity equation has to be solved as a first step in the modeling process,

$$\Delta\hat{n} - \frac{\hat{n}}{\tau_{\text{n}} D_{\text{n}}} + \frac{G(x,y,z)}{D_{\text{n}}} = 0 \tag{2}$$

where $\hat{n}$ is the three dimensional excess carrier concentration, $D_{\text{n}}$ and $\tau_{\text{n}}$ are the electron diffusion coefficient and lifetime, and $G(x,y,z)$ is the optical generation rate, i.e. the number of photogenerated electron-hole pairs per unit volume and time. In the case of light impinging vertically over the photosensing surface and considering the coordinate system in Fig. 1, we write,

$$G(y) = -\frac{\partial \Phi(y)}{\partial y} \tag{3}$$

where $\Phi(y)$ is the photon flux. According to Beer's law, the photon flux decreases exponentially with $y$ (penetration depth in Si) as $\Phi(y) = \Phi_0 e^{-\alpha y}$, where $\alpha$ is the absorption coefficient and $\Phi_0$ is the photon flux at the silicon surface, $\Phi_0 = \frac{P_{\text{opt}} T \lambda}{hc}$, where $P_{\text{opt}}$ stands for the incident optical power, $T$ is the transmission coefficient, $h$ the Planck's constant, $\lambda$ the impinging radiation wavelength and $c$ the speed of light.

### *A. 1D models*

One of the first analytical models for photodiodes based on the solution of the steady-state continuity equation dates from 1977, [23]. Although the study focuses on small photodiodes for its time, their 50-200 $\mu$m wide size will make them bulky for nowadays standards. Besides, the device considered is an InSb p-$n^+$ mesa photodiode whose structure imposes particular boundary conditions, and the study is limited to the substrate. In this paper, a 1D approximation is proposed that, particularized for a p-$n^+$ photodiode such as the one in Fig. 1(a), results in, [23],

$$I = q\frac{x_{ph}}{2}\phi_0 e^{-\alpha(y_j+W)}\frac{\alpha}{\alpha + (1/L_n)} \tag{4}$$

Despite its limitations, this work constitutes to the best of our knowledge the first attempt to study the peripheral photocurrent and its dependence on parameters such as the minority carrier diffusion length and the surface recombination velocity. Although a two-dimensional analysis is attempted in this paper, the resulting system is deemed to large to be solved

explicitly and a numerical approach is used instead which is compared to the one-dimensional approximation shown above.

More recent studies include fairly elemental 1D models in SPICE. A photodiode model for DC as well as high frequency circuit simulation was presented in [34]. The photocurrent is given by a very simple expression in terms of the quantum efficiency, $\eta$, as, [34],

$$I = \frac{\eta\, q\, \lambda \phi}{h\, c} \tag{5}$$

The accuracy of the model was verified with the measured data obtained from p-n$^+$ and p-n$_{\text{well}}$ photodiodes fabricated using a conventional 0.25 $\mu$m CMOS technology. The devices considered, however, have a diameter of 75 $\mu$m, large enough to conceal peripheral effects. Another analytical model for PSPICE simulation was developed in [35]. Both n-p$_{\text{sub}}$ and p$^+$-n$_{\text{well}}$ structures were studied by solving the steady-state response. In the case of the n-p$_{\text{sub}}$ photodiode the derived expression reported is, [35],

$$\begin{aligned} J = & \frac{q\, \phi_0\, L_p}{1-(\alpha\, L_p)^2} \left( \alpha\, L_p\, e^{-\alpha\, y_j} + \sinh \frac{y_j}{L_p} \right. \\ & \left. + A(x_j, L_p) \cosh \frac{y_j}{L_p} \right) + q \frac{\phi_0}{\alpha} \left(1 - e^{-\alpha W}\right) e^{-\alpha y_j} \\ & + \frac{q\, \phi_0\, L_n}{(\alpha L_n)^2 - 1} \left( A(y_w - (y_j + W), L_n) + \alpha L_n \right) e^{-\alpha (y_j + W)} \end{aligned} \tag{6}$$

where $D_p$ and $L_p$ are the hole diffusion coefficient and length, respectively, and the function $A(x, L)$ is needed to satisfy boundary conditions, [35]. The model was verified for a large 1cm$^2$ area device by comparing the PSPICE circuit simulations to results from the Medici numerical semiconductor device simulator. More useful models are found in [36] and [37]. In both papers the steady-state continuity equation is solved in the different regions of the device under similar boundary conditions. In the former, p-epi-n$_{\text{well}}$ and p-epi-p$_{\text{well}}$-n$^+$ photodiodes were considered and an expression for the total current density in terms of the drift and diffusion components is outlined but not explicitly derived. Fabricated devices in a TSMC 0.5 $\mu$m CMOS technology were used to study the effect of the surface recombination velocity in order to avoid an inadequate value affected by the surface defects in the manufacture process. The latter presents the definition and implementation of a n-p$^+$ photodiode current density model, [37],

$$\begin{aligned} J = & q\, D_p \left( -k_p \alpha\, e^{-\alpha (y_j + W)} - \frac{C_1}{L_p} e^{-(y_j + W)/L_p} \right. \\ & \left. + \frac{C_2}{L_p} e^{(y_j + W)/L_p} \right) \\ & + q\, D_n \left( -k_n \alpha\, e^{-\alpha y_j} - \frac{C_3}{L_n} e^{-y_j/L_n} + \frac{C_4}{L_n} e^{y_j/L_n} \right) \\ & + q\, \phi_0\, e^{-\alpha y_j} \left(1 - e^{-\alpha\, W}\right) \end{aligned} \tag{7}$$

where $C_1$, $C_2$, $C_3$ and $C_4$ are coefficients extracted from the particular boundary conditions, [37]. This model was validated by comparison with numerical device simulations using DESSIS of ISE-TCAD. Simulation results were also compared with experimental data from a p-n$^+$ photodiode including a $SiO_2$-$Si_3N_4$ antireflecting coating optimized for near-infrared applications and a PIN photodiode for X-ray imaging applications.

### *B. 2D models*

All the previous models neither include an analytical solution of the peripheral photocurrent nor mention it, except for [23]. Taking this phenomenon into account requires at least a two-dimensional treatment of the steady-state continuity equation, which constitutes a challenge from a mathematical point of view. Next, the main studies on the 2D peripheral collection with varying approaches over mesa, lateral, finger, and backside illuminated photodiodes apart from vertical ones will be summarized.

An array of p-n lateral finger photodiodes was studied in [24]. Two basic geometries are considered, an array of uniformly spaced narrow stripe collectors and a hexagonal matrix of small circular collectors. In the case of the stripe collectors, the symmetry of the structure, in addition to other assumptions, simplifies the calculation of the lateral collection. In particular, the term in the diffusion equation representing the variation of the diffusion current flowing in the vertical direction is neglected and a constant optical generation rate is assumed. Consequently, the diffusion equation is effectively reduced to one dimension, and the laterally collected current density is given by the following equation, [24],

$$J = q\, G\, L_n\, \tanh \left( \frac{x_l - x_{ph}}{2 L_n} \right) \tag{8}$$

In the case of the matrix of circular collectors, an expression of the total photocurrent as a function of modified Bessel and Hankel functions is given.

Few years later, the same authors presented a theory for the enhanced photoresponse of p-n junctions that arises from the lateral diffusion of photogenerated carriers, [25]. In this model, the p-n junction is fabricated in a periodical mesa structure, which imposes particular boundary conditions. The solution is a complex set of relations which are more useful by considering some special cases. These particular solutions are compared with the results of numerical analysis. It was found that the magnitude of the peripheral photoresponse is sensitive to geometric and physical factors such as semiconductor thickness, surface recombination, optical absorption length, and competition for photogenerated carriers by adjacent photodiodes. Moreover, an increase of the lateral collection significance for smaller devices is predicted. Lateral photodiodes were also the subject of study in [38], where a circuital model was proposed. The resolution of the continuity equation in this case was divided in two parts: an electrical solution, which corresponds to the one-dimensional solution without generation term, and a photonic solution, which represents the two-dimensional solution with the generation term. The results are compared to an approximated one-dimensional classical approach confirming that a two-dimensional model is needed. The continuity equation for generated carriers

within a two-dimensional structure was also solved in [39] to develop an analytical model for finger p-NBL(N-Buried-Layer)-$p_{well}$-$n^+$ photodiodes. Simplifying assumptions were introduced for each of the device regions as, for instance, the no $y$-dependence in the N-Buried-Layer and P-substrate. The continuity equation was solved in the $n^+$ region applying the technique of separation of variables and the same procedure is supposedly used for the $p_{well}$ between two $n^+$ diffusions, although the solution is not reported. Numerical device simulations from ATLAS show good agreement with the carrier concentration given by the model, which was also successfully compared with measurements of the structure under consideration fabricated in a 0.6 $\mu$m BiCMOS process.

Although the previous two-dimensional models are of interest because they deal with the peripheral phenomenon in different ways, they are specific for lateral, mesa and finger structures. In order to broaden our study, three different works dealing with vertical photodiodes were included. In [40], a quantitative description of the photocurrent of a p-$n^+$ photodiode was developed based on [24], particularized for the case of a thin film substrate. The analysis makes use of the fact that the current density at the peripheral edges of the photodiode in a closely spaced array has a maximum value near the surface and decays approximately in a linear fashion with the depth into the substrate. Simulation data of the current density using Davinci$^{TM}$ are used to prove this assumption. Finally, the photocurrent given by experimental measurements in a 0.5 $\mu$m CMOS technology is compared with the derived expression, demonstrating that the correspondence improves due to the lateral collection.

Beyond the previous current determination quantitative approach, an analytical charge collection model was derived in [41] to assess the impact of the photodiode size, doping profile and surface recombination velocity on the Modulation Transfer Function (MTF) and on the charge collection efficiency of a p-$n^+$ junction. The transmittance is considered as unity and the photogeneration function includes a sinusoidal term to facilitate MTF extraction. Additional symmetry conditions are imposed in order to use Green's functions to solve the two-dimensional steady-state continuity equation. Although the calculated MTF results agree well with measured data of fabricated imagers based on three different pixel designs in a 0.5 $\mu$m CMOS process, the final expression is only barely outlined and cannot be easily used. MTF modelling was also considered in [42]. In this case, the model is based on the solution of the two-dimensional diffusion equation and covers the impact of the pixel active area geometrical shape. However, the two-dimensional analysis is limited to the substrate under the diffusion area and the contribution of lateral photocarriers is not taken into account. The theoretical prediction is compared with results obtained by means of a sub-micron scanning system from $p_{well}$-$n^+$ photodiode APSs fabricated in a standard CMOS 0.35 $\mu$m technology.

The two-dimensional diffusion equation of photocarriers was solved numerically for long wavelength infrared 2D arrays of backside illuminated photovoltaic diodes, [46], [47]. The calculations take into account both the thermally and optically generated carriers originated under the junction and those originated from around the junction. The results show that there is an optimum photodiode size that maximizes the quantum efficiency while minimizing crosstalk.

### *C. 3D models*

Finally, there are very few works which tackle the problem of the three-dimensional continuity equation resolution. In [26], the self- and cross-responsivities of n-$p^+$ photodetector arrays are described by a three-dimensional analytical model based on Fourier series under the constraints of periodic illumination and a mesa structure. The photocurrent and the crosstalk are obtained from the ambipolar transport equation,

$$\frac{\partial \hat{n}}{\partial t} = D_a \nabla^2 \hat{n} + \mu_a \vec{E}\, \vec{\nabla} \hat{n} - \frac{\hat{n}}{\tau} + G(x,y,z,t) \qquad (9)$$

where $\hat{n}(x,y,z,t)$ is the excess carrier distribution and $D_a$ and $\mu_a$ are the ambipolar diffusion coefficient and mobility, respectively. The work focuses on the substrate and the symmetry implies particular boundary conditions. Also, in order to reach a fully analytical solution, the spacing between the adjacent elements was supposed to be small compared with their length and width. Under this assumption, compact expressions can only be obtained for particular cases such as in the case of a photodiode with a semi-infinite substrate. In this case, the photocurrent generated by monochromatic incident radiation and collected by a rectangle $(x_2 - x_1)(y_2 - y_1)$ at the bottom edge of the depletion region, assuming square photodiodes, is given by,

$$I = \alpha\, \phi_0 \left( \frac{x_{ph}^2 (x_2 - x_1)(y_2 - y_1)}{4L^2(\alpha^2 - 1/L_n^2)} + F(x_1, x_2, y_1, y_2) \right) \qquad (10)$$

where $L$ is the spatial period of the illumination function and $F(x_1, x_2, y_1, y_2)$ is a function build from Fourier series, [26]. The accuracy of the predictions was proved using measured data for HgCdTe and InSb photodiodes. Based on this work, a three-dimensional model was presented in [43], as the second part of a work in which a one-dimensional analysis of $p^+$-epi-$n^+$ photodiodes was derived, [44]. The analytical solution was verified with numerical simulations using Medici and based on parameters extracted from a standard 0.35 $\mu$m CMOS process. In the second part of the paper, investigation of lateral photoresponse using linear photodiode arrays and numerical device simulations was presented, illustrating the importance of surface recombination and mobility degradation along the Si-$SiO_2$ interface. For the sake of obtaining an analytical solution, the same assumption as in [26] regarding the spacing of the photodiodes is made, although the authors point out that at large photodiode separation distances the neglected mobility degradation along the z = 0 plane somewhat offsets the underestimation resulting from this assumption.

A general and fully analytical three-dimensional model that describes the lateral collection through the side-walls of the junction of a single CMOS photodiode operating in the visible range was developed in [45], [50]. In this case, although the continuity equation for minority carriers is solved in two dimensions, the result is then integrated to 3D in order to

evaluate the behavior of the whole device. The model accounts for surface recombination effects through the definition of appropriate boundary conditions. It also assumes uniform illumination conditions of a single photodiode and therefore, considerations of lateral crosstalk do not apply in this case. The total steady-state current of the photodiode in the reverse operation regime comprises three main components. First, $I_{\rm aa}$, the active area current generated by the diffusion of minority carriers and generation of electron-hole pairs in the depletion region, including the collection through the bottom of the depletion region due to the carriers generated deep in the substrate,

$$I_{\rm aa} = q x_{\rm ph}^2 \left( \int_0^{y_{\rm j}+W} G(y) {\rm d}y + D_{\rm n} \left. \frac{\partial n_{\rm p}}{\partial y} \right|_{y_{\rm j}+W} - D_{\rm p} \left. \frac{\partial p_{\rm n}}{\partial y} \right|_{y_{\rm j}} \right) \quad (11)$$

In the case of p-n$_{\rm well}$ photodiodes, the introduction of the well modifies $I_{\rm aa}$ adding one extra component identical to (11) where $x_{\rm ph}^2$ is substituted by $x_{\rm well}^2$ and the minority hole concentration in the well surrounding the diffusion is considered. Second, $I_{\rm W}$, the drift current generated in the lateral depletion region. This component can be found by integrating the generation rate over the whole region formed by the $s$ sides of the polygonal junction (in the case of Fig. 1 $s$ equals 4), but proved out to be not very significant.

$$I_{\rm W} = s\, q\, x_{\rm ph} \int_0^{W_\ell} \int_0^{y_{\rm j}+W} G(y) {\rm d}y\, {\rm d}x \quad (12)$$

The same expression is obtained in the case of p-n$_{\rm well}$ photodiodes substituting $x_{\rm ph}$ by $x_{\rm well}$. Finally, $I_{\rm lateral}$, the lateral current generated in the surroundings of the photodiode by minority carriers that reach the junction by diffusion. This phenomenon is more pronounced in small photodiodes due to the increase of the ratio of the total lateral area to the active area, in this case $I_{\rm lateral}$ is comparable to the active area current $I_{\rm aa}$, showing a strong dependence with the active area to surrounding area ratio. The calculation of this term constitutes a non-homogeneous problem which can be solved applying the method of separation of variables, [45], [51], yielding,

$$I_{\rm lateral} = s \frac{2 x_{\rm ph} q D_{\rm n}}{y_{\rm w}} \sum_{n=1}^{\infty} I_1(y_{\rm w})\, I_2(x_{\rm s})\, I_3(y_{\rm j}) \quad (13)$$

where

$$\begin{aligned} I_1(y_{\rm w}) &= (-1)^n \Bigg[ -\frac{\gamma \frac{D_{\rm n}}{S_{\rm n}} \cosh\left(\frac{y_{\rm w}}{L_{\rm n}}\right)}{\sigma_{\rm n}} + \\ &\quad + \frac{\frac{\alpha\, \phi_0}{D_n}}{\frac{1}{L_{\rm n}^2} - \alpha^2} \left( \frac{\cosh\left(\frac{y_{\rm w}}{L_{\rm n}}\right) - e^{-\alpha y_{\rm w}}}{\sigma_{\rm n}} - \frac{\sinh(\alpha y_{\rm w})}{\alpha^2 + \theta_{\rm n}^2} \right) \Bigg] \\ I_2(x_{\rm s}) &= \frac{\sqrt{\sigma_{\rm n}} \left(1 - \cosh\left(\sqrt{\sigma_{\rm n}} x_{\rm s}\right)\right)}{\sinh\left(\sqrt{\sigma_{\rm n}} x_{\rm s}\right)} \\ I_3(y_{\rm j}) &= 1 - \cos(\theta_{\rm n} y_{\rm j}) \end{aligned} \quad (14)$$

where $S_n$ is the surface recombination velocity and $\theta_{\rm n} = n\,\pi/y_w$ and $\sigma$ is a separation constant, [45]. In the case of p-n$_{\rm well}$ photodiodes, an identical expression is found with $x_{\rm well}$ instead of $x_{\rm ph}$, but in this case a second contribution to the lateral photocurrent due to photocarriers in the surrounding volume which does not form p-n junctions with the well must be added. Device simulations showed that this contribution is not negligible and can be modeled as $I_{\rm lateral} x_s / x_{\rm well}$, [52].

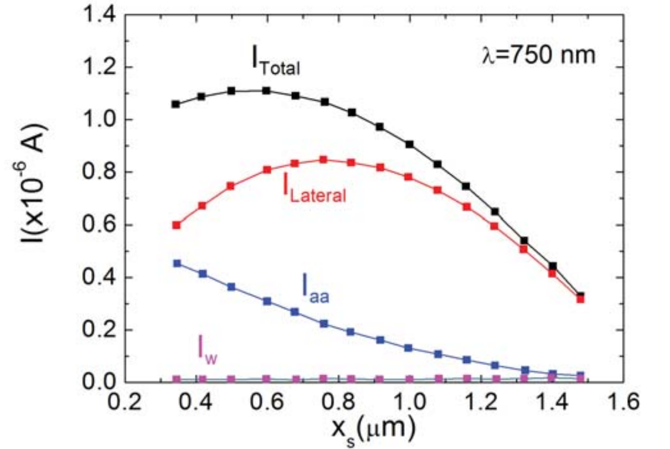


Fig. 2. Current components when p-n$^+$ photodiodes with different values of $x_{\rm ph}$ ranging from 0.44 $\mu$m to 2.7 $\mu$m within a cell of fixed size of $x_\ell^2 = 4 \times 4 \mu{\rm m}^2$ are illuminated with monochromatic light of $\lambda = 750$nm.

In order to state the relative importance of the lateral contribution on the overall photocurrent, we consider the case of a p-n$^+$ junction in which the whole device area is uniformly illuminated. We consider a unique cell of size $x_\ell^2 = 4 \times 4 \mu{\rm m}^2$ and different values of $x_{\rm ph}$ ranging from 0.44 $\mu$m to 2.7 $\mu$m, resulting in a varying $x_{\rm s}$. Fig. 2 plots the different components of the photocurrent, including the total current,

$$I_{\rm total} = I_{\rm lateral} + I_{\rm aa} + I_{\rm W} \quad (15)$$

As can be seen, the lateral collection represents a significant part of the total photocurrent through the device. It is also worth mentioning that the dependence of the lateral current on the collecting area surrounding the device, through the parameter $x_{\rm s}$, results in the existence of a maximum response in the total current for such small photodiodes. The same behaviour was found independently of the wavelength in the visible range. This result has been confirmed by experimental data from isolated square p-n$^+$ photodiodes of different sizes fabricated in $0.18 \mu$m and 65 nm CMOS standard technologies, where different photosensing structures were used in order to independently characterize the total and lateral photocurrent [53]. Individual photodiodes are widely spaced to avoid interferences, as shown in Fig. 3, and directly connected to raw pads without ESD protection to prevent the appearance of coupling capacitances. Experimental results in a standard CMOS 65nm technology are shown in Table I, where the percentage contribution of the lateral component with respect to the total photocurrent is shown. Inspection of the data confirms that for small photodiodes the lateral current dominates the total current as predicted by the model. In fact, for small photodiodes and large lateral space available , $x_{\rm s} + W_\ell$,

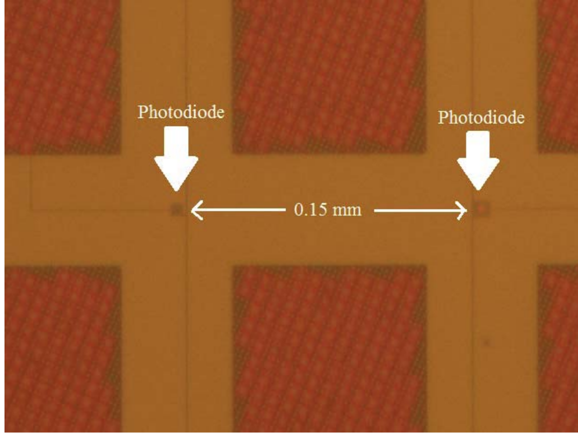


Fig. 3. Microphotograph showing the separation between the p-n$^+$ photodiodes.

TABLE I
$\frac{I_{\text{LATERAL}}}{I_{total}} \times 100$, PERCENTAGE OF LATERAL CONTRIBUTION IN P-N$^+$ PHOTODIODES FABRICATED IN A STANDARD CMOS 65NM PROCESS FOR $\lambda = 532$ NM.

| | $x_s + W_\ell$ ($\mu$m) | | | | | |
|---|---|---|---|---|---|---|
| $x_{ph}$ ($\mu$m) | 0.355 | 0.605 | 0.855 | 1.105 | 1.355 | 1.605 |
| 0.56 | 95% | 95% | 88% | 88% | ≈100% | ≈100% |
| 1.06 | 90% | 97% | 92% | 92% | 87% | 92% |
| 1.56 | 90% | 94% | 91% | 93% | 92% | - |
| 2.06 | 88% | 90% | 88% | 87% | 89% | - |
| 2.56 | 80% | 84% | 86% | 81% | 75% | - |
| 3.06 | 82% | 75% | - | - | - | - |

this contribution adds up to almost the totality of the device photocurrent. Also, in general terms, for a given lateral space available the bigger the photodiode active area the smaller the contribution of the lateral term to the total photocurrent. This is a general trend to be considered within reasonable variability concerns.

A more qualitative analysis is made in Fig. 4, where the measured lateral photocurrent of p-n$^+$ photodiodes fabricated in two different CMOS process technologies for two different wavelengths is represented with respect to the distance between the edge of the depletion region and the lateral limit of the photodiode, $x_s$, and compared to the analytical model in [45]. As seen, the analytical model fits well the experimental data and constitutes a powerful tool to maximize the photoresponse while optimizing the total layout area cost. This knowledge is of particular importance for sub-100nm technologies as published experimental data are scarce.

Similar results can be found in p-n$_{\text{well}}$ photodiodes, as shown in Fig. 5 where 3D numerical device simulations are compared with the modeled results of the different components of the main photocurrent, $I_{\text{total}}$. The model fits the simulated data reasonably well with a minor disagreement in the active area current component for photodiodes with wide wells. The lateral contribution from photocarriers generated in the part of the surrounding substrate not forming lateral p-n junctions which, as explained before, follows the pattern $I_{\text{lateral}}\, x_{\text{s}}/x_{\text{well}}$, is not negligible and even matches the lateral component due to the p-n junctions for photodiodes with small active area. The

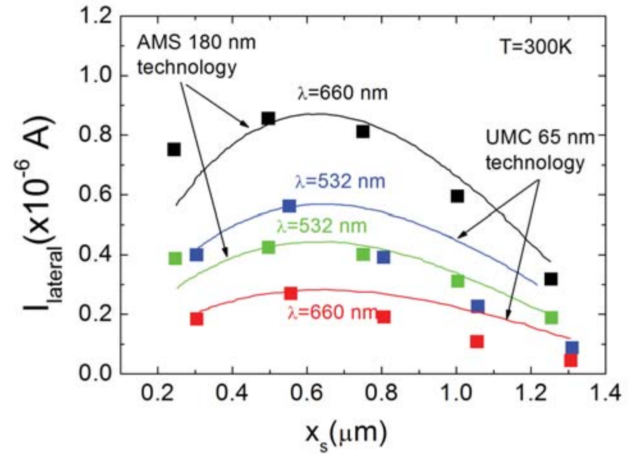


Fig. 4. Comparison of experimental data of p-n$^+$ photodiodes in CMOS 180 nm and 65 nm processes (symbols) with the analytical model (shown in solid lines) in [45] for different wavelengths as a function of the distance between the limit of the depletion region and the photodiode, $x_s$, for $W_l = 0.05\mu m$ and $x_l = 3.27\mu m$.

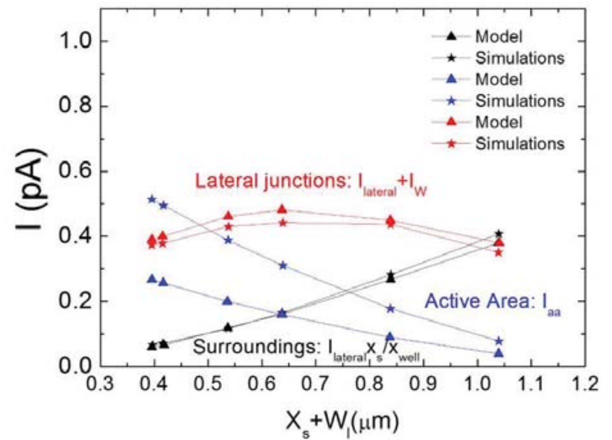


Fig. 5. Comparison between the simulated and modeled components of $I_{\text{total}}$ for p-n$_{\text{well}}$ photodiodes versus different $x_s$ values under a 550nm light source.

disagreement in the $I_{\text{aa}}$ calculation at lowest $x_{\text{s}}$ values does not compromise the model usefulness because it coincides with the technological limit, which does not allow smaller $x_{\text{s}}$ values.

Taking advantage of the compact and explicit nature of this model, it is possible to use the potential offered by current hardware description languages (HDLs) in the mixed signal domain such as VHDL-AMS and Verilog-AMS to perform circuit-level simulations of imager devices in standard CAD tools, [54]. Compared to SPICE language for circuit simulation, HDLs offer some benefits as, for example, the incorporation of non-electrical mechanisms as far as they can be described through mathematical expressions. Additionally, the use of appropriate compilers guarantees that the models can be directly interfaced with any circuit simulator.

In the last decade, several works dealing with photodiode models in HDL have been published. In [55] some models

for optoelectronic devices are presented, including one for a commercial high speed InGaAs PIN photodiode in VHDL-AMS. Although the mathematical expressions are not reported, this work constitutes a good example of the HDLs potential. In [56], a Verilog-A photodiode model is presented that does not explicitly reflect physical and technological parameters. In addition, it requires a careful a priori process of characterization and parameter extraction before being used as a design element. Finally, several photodetectors and pixel sensors are modelled with VHDL-AMS in [57] and [58], respectively, but the mathematical models follow classical expressions. All these models fail to include lateral effects.

An example of the convenience of the implementation of (15) in a HDL can be seen in Fig. 6, where circuit simulations for a standard 3T-APS pixel such as the one in Fig. 6(a) were performed with the same photodiode total area $x_\ell^2$ and different values of the active area $x_{\text{ph}}^2$ under a light source with $P_{\text{opt}} = 5 \cdot 10^4$ W/m$^2$ and $\lambda = 550$ nm, Fig. 6(b). As can be observed, even for a fixed total area, different active area sizes correspond to different pixel sensitivities given by the slope of the curve. The $V_{\text{out}}(t)$ curve with the maximum slope, corresponding to devices with $x_{\text{ph}}^2 = 3.53\mu\text{m}^2$, represents the best photodiode response, which does not correspond with the maximum size of the n$^+$ diffusion, $x_{\text{ph}}^2$. Consequently, the results confirm that when the lateral effects are taken into consideration there is an optimum active area which maximizes the rate of decay of $V_{\text{out}}$ and hence the pixel sensitivity. This kind of circuit-level analysis would not be possible without compact and explicit photodiode models valid for HDL implementation.

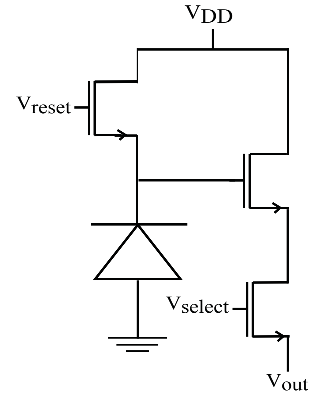


(a) 3-transistor APS pixel cell

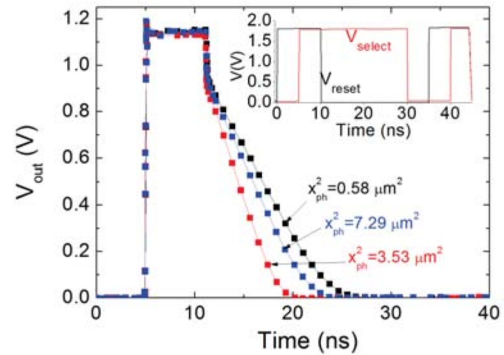


(b) Output voltage versus time for different $x_{\text{ph}}$ values.

Fig. 6. Circuit simulations with $\lambda = 550$ nm and $P_{\text{opt}} = 5 \cdot 10^4$ W/m$^2$ of a 3T-APS pixel using a HDL description of the photocurrent model in (15) to assess the effect of the photodiode geometry in the overall pixel sensitivity.

## V. Crosstalk

The photocarriers produced by illumination in the photodiodes surrounding the device under study produce differences in the output signal with respect to an isolated photodiode. These differences are usually named crosstalk (CTK). An optical and an electrical component can be studied to characterize CTK effects. The optical component is linked to illumination that reaches the photodiode surface but penetrates other neighboring devices due to the rays inclination or different effects connected with microlenses. The electrical component, the one considered here, is always found in conventionally fabricated CMOS image sensors; it takes into consideration the diffusion of photocarriers coming from neighboring photodiodes. Unfortunately, the only way to reduce the optical and electrical CTK components involves substantial technological changes on CMOS imagers standard processes [59]. In addition to the previously explained dependencies, CMOS image sensors CTK effects are connected with pixel location in the pixel array layout; therefore, it depends on the particular location of the photodiode and the electronics in the pixel area. CTK effects also depend on the pixel size (apart from geometrical considerations) [27], [29], [60], that is why CTK rises as scaling advances in the CMOS image sensor context [61].

The conventional methods to characterize photodiode operation are not adequate for CTK effects; to do so, there are two possibilities available. In order to avoid light penetration in certain pixels, masks can be used and illumination can be measured in unmasked pixels, [62]. In addition, the spot-scanning technique can be employed, where an individual pixel is illuminated in order to measure the corresponding effects in the neighboring devices, [63]. The masking technique can be affected by diffraction effects and the spot-scanning methods need a reduced enough laser spot for small pixels characterization. All these subtleties pose important difficulties in CTK characterization, being this the reason why device simulation and physical modeling can be of great help to deal with this issue, [64], [65].

Prototypes fabrication costs can be reduced by means of design optimization through the use of compact models, that is why there exist a great pressure to increase efforts in this direction. The models, as a general rule, are required to be physically based, analytical and explicit. This is no easy task because of the different configurations, fabrication processes and geometrical considerations linked to the CMOS image sensor industry, as all this reflects on CTK effects. In order to develop current models including CTK effects we have to take into account two important issues. On the one hand, the worst scenario in terms of CTK modeling takes place when

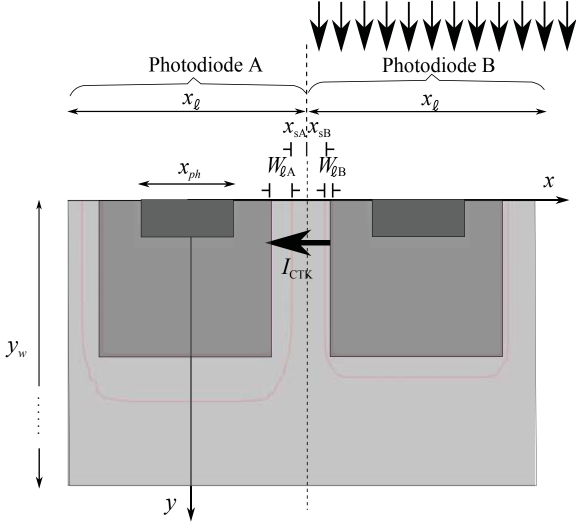


Fig. 7. Cross section of the photodiode of interest, A (left) and its neighbor B under illumination (right). $W_{\ell \mathrm{A,B}}$ represent the lateral width of the depletion region of photodiodes A and B; $x_{s\mathrm{A,B}}$ represent the distance between the edge of the depletion region and the lateral limit of photodiodes A and B respectively. Other geometrical parameters of these photodiodes are similar to those given in Fig.1.

two neighboring photodiodes are placed together with no in-pixel electronics in-between [66]. On the other hand, due to the inherent bi-dimensional nature of light propagation and carrier diffusion in semiconductor devices, a two dimensional model is needed to accurately account for the physics within the photodiodes. Taking into consideration the results reported in the previous sections in relation to the needed trade-off between the peripheral and active area current contributions in highly scaled devices, this latter issue becomes essential. One of the most interesting models reported so far on this issue is given in [29]. It consists of an approximation related to the pixel geometrical shape and it is presented within a semianalytical approach. Another previously proposed model makes use of an analytical equation although no lateral diffusion is considered because of changes in a standard fabrication process [67], consequently CTK effects are probably underestimated. In spite of the models commented above, it is important to highlight that there is an important lack of CTK models in the literature.

Crosstalk can be calculated as follows,

$$\mathrm{CTK}\,(\%) = \frac{I_\mathrm{n}}{I_\mathrm{total}} \times 100 \tag{16}$$

where $I_\mathrm{total}$, described in (15), stands for the total photodiode current under the illumination conditions , and $I_\mathrm{n}$ accounts for the measured photocurrent in a device linked to the effects of a similar illumination on an identical neighbor. Both currents ($I_\mathrm{total}$ and $I_\mathrm{n}$) are measured in the reverse-biased photodiode under study. Fig. 7 shows the cross-section of the structure under study here where subscript A (left) represents the photodiode of interest, which is reverse-biased, and B (right), the photodiode under illumination, is its zero-biased neighbor. The geometrical parameters which describe both structures are also indicated.

Analytical models for $I_\mathrm{total}$ have already been presented for both p-n and p-$\mathrm{n_{well}}$ photodiodes in Section IV-C. A parallel process leads to an analytical expression for $I_\mathrm{n}$ accounting for the neighboring photodiodes, [52], [68]. The current is obtained considering two terms: the saturation current of the reverse-biased diode A, $I_\mathrm{o}$, and the CTK lateral current related to generated carriers in the surroundings of neighbor B which is zero-biased and under illumination, $I_\mathrm{CTK}$,

$$I_\mathrm{n} = I_\mathrm{o} + I_\mathrm{CTK} \tag{17}$$

The continuity equation in the steady-state regime has to be solved to determine the minority carrier distribution in the surroundings of photodiode A,

$$\frac{\partial^2 \hat{n}_\mathrm{A}}{\partial x^2} + \frac{\partial^2 \hat{n}_\mathrm{A}}{\partial y^2} - \frac{\hat{n}_\mathrm{A}}{L_\mathrm{n}^2} = 0 \tag{18}$$

accounting for the boundary conditions below

$$\begin{aligned} \hat{n}_\mathrm{A}(x,0) &= \gamma_\mathrm{A}\frac{D_\mathrm{n}}{S_\mathrm{n}} \\ \hat{n}_\mathrm{A}\left(\frac{x_\mathrm{ph}}{2} + W_{\ell_\mathrm{A}}, y\right) &= -n_\mathrm{p0} \\ \hat{n}_\mathrm{A}(x, y_\mathrm{w}) &= 0 \\ \hat{n}_\mathrm{A}\left(\frac{x_\ell}{2}, y\right) &= \hat{n}_\mathrm{CTK}(y) \end{aligned} \tag{19}$$

where $\hat{n}_\mathrm{A}$ stands for the excess electron concentration in photodiode A. A fitting parameter ($\gamma_\mathrm{A}$) is employed following the approach sketched in [53]. $\hat{n}_\mathrm{CTK}(y)$ represents the distribution of excess minority carriers due to the illumination in photodiode B in the boundary between the devices. The solution of the stationary continuity equation in the neighbor surroundings allows the determination of the previous quantity,

$$\frac{\partial^2 \hat{n}_\mathrm{B}}{\partial x^2} + \frac{\partial^2 \hat{n}_\mathrm{B}}{\partial y^2} - \frac{\hat{n}_\mathrm{B}}{L_\mathrm{n}^2} = -\frac{G(y)}{D_\mathrm{n}} \tag{20}$$

using as boundary conditions the following equations,

$$\begin{aligned} \hat{n}_\mathrm{B}(x,0) &= \gamma_\mathrm{B}\frac{D_\mathrm{n}}{S_\mathrm{n}} \\ \hat{n}_\mathrm{B}\left(x_\ell - \frac{x_\mathrm{ph}}{2} - W_{\ell_\mathrm{B}}, y\right) &= 0 \\ \hat{n}_\mathrm{B}(x, y_\mathrm{w}) &= 0 \\ \hat{n}_\mathrm{B}\left(\frac{x_\ell}{2}, y\right) &= \hat{n}_\mathrm{CTK}(y) \end{aligned} \tag{21}$$

where $\hat{n}_\mathrm{B}$ stands for photodiode B excess electron concentration.

At the boundary of photodiode B depletion region, the current density in the x-direction is negligible and, therefore,

$$J_\mathrm{nB}\left(x_\ell - \frac{x_\mathrm{ph}}{2} - W_{\ell_\mathrm{B}}, y\right) = qD_\mathrm{n}\frac{\partial \hat{n}_\mathrm{B}(x,y)}{\partial x}\bigg|_{x_\ell - \frac{x_\mathrm{ph}}{2} - W_{\ell_\mathrm{B}}} = 0 \tag{22}$$

Making use of the boundary conditions (19) and (21), equations (18) and (20) can be solved by a separation of variables procedure. In this manner, the lateral current component connected to CTK effects can be obtained by integration of

the current density at the depletion region over the side-wall boundary as follows,

$$I_{\text{CTK}} = \int_{-\frac{x_{\text{ph}}}{2}}^{\frac{x_{\text{ph}}}{2}} \int_{0}^{y_{\text{j}}} J_{\text{nA}} \left( \frac{x_{\text{ph}}}{2} + W_{\ell_{\text{A}}}, y \right) \text{d}y\text{d}z \tag{23}$$

the result is given below,

$$I_{\text{CTK}} = x_{\text{ph}} q D_{\text{n}} \sum_{n=1}^{\infty} \frac{\sqrt{\sigma_n}}{\theta_n} \times \left( \frac{V_{\text{B}} \left( \cosh\left(\sqrt{\sigma_n} x_{\text{sB}}\right) - 1 \right) + V_{\text{A}} \left( 1 - \cosh\left(\sqrt{\sigma_n} x_{\text{sA}}\right) \right)}{\sinh\left(\sqrt{\sigma_n} x_{\text{sA}}\right)} \right) \times \left(1 - \cos(\theta_n y_{\text{j}})\right) \tag{24}$$

where

$$V_{\text{A}} = -\frac{2(-1)^n \theta_n}{y_{\text{w}}} \frac{\gamma_{\text{A}} D_{\text{n}}}{S_{\text{n}} \sigma_n} \cosh\left(\frac{y_{\text{w}}}{L_{\text{n}}}\right) \tag{25}$$

$$V_{\text{B}} = -\frac{2(-1)^n \theta_n}{y_{\text{w}}} \left( \frac{\gamma_{\text{B}} D_{\text{n}}}{S_{\text{n}} \sigma_n} \cosh\left(\frac{y_{\text{w}}}{L_{\text{n}}}\right) + \frac{\frac{\Phi_0 \alpha}{D_{\text{n}}}}{\frac{1}{L_{\text{n}}^2} - \alpha^2} \left( \frac{\sinh(\alpha y_{\text{w}})}{\alpha^2 + \theta_n^2} - \frac{\cosh\left(\frac{y_{\text{w}}}{L_{\text{n}}}\right) - e^{-\alpha y_{\text{w}}}}{\sigma_n} \right) \right) \tag{26}$$

with $x_{\text{sA,B}} = \frac{x_\ell}{2} - \frac{x_{\text{ph}}}{2} - W_{\ell_{\text{A,B}}}$.

Taking into account that $n=1$ is appropriate, the summation in (24) can be simplified. The same expression holds for both p-n and p-n$_{\text{well}}$ photodiodes substituting $x_{\text{ph}}$ by $x_{\text{well}}$ in (24).

Considering the photodiode model reported previously [45], and the modeled CTK current component, the final expression for the CTK model can be obtained,

$$\text{CTK}\,(\%) = \frac{I_{\text{o}} + I_{\text{CTK}}}{I_{\text{aa}} + I_{\text{W}} + I_{\text{lateral}}} \times 100 \tag{27}$$

The expressions developed for the CTK allowed us to reproduce both experimental measurements and simulation data obtained for a copious variety of geometrical parameters and illumination wavelengths in the photodiodes under study for both p-n$^+$ and p-n$_{\text{well}}$ photodiodes, [52], [68]. A comparison between a p-n$_{\text{well}}$ ($x_{\text{well}} = 3.06$ $\mu$m, $x_{ph} = 1.06$ $\mu$m) and a p-n$^+$ photodiode with a diffusion of the same size of the well ($x_{ph} = 3.06$ $\mu$m), and the same total width, $x_\ell = 5.06$ $\mu$m, with uniform illumination, in the visible range and beyond, for a standard 180 nm technology can be seen in Fig. 8. We have plotted $I_{\text{total}}$ (main photocurrent obtained by illumination of photodiode A) and $I_{\text{n}}$ (crosstalk component obtained by illumination of zero-biased photodiode B ($x_\ell/2 \le x \le 3x_\ell/2, -x_\ell/2 \le z \le x_\ell/2$)), as given in Fig. 7. We can see that for p-n$_{\text{well}}$ photodiodes $I_{\text{total}}$ and $I_{\text{n}}$ are bigger than in the p-n$^+$ case, in the visible range mostly. Also, the maximum response takes place at longer wavelenghts in comparison with p-n$^+$ photodiodes. The previous results show a better CTK response for wavelenghs below $\lambda = 700$ nm, for higher wavelenghts there are no important differences.

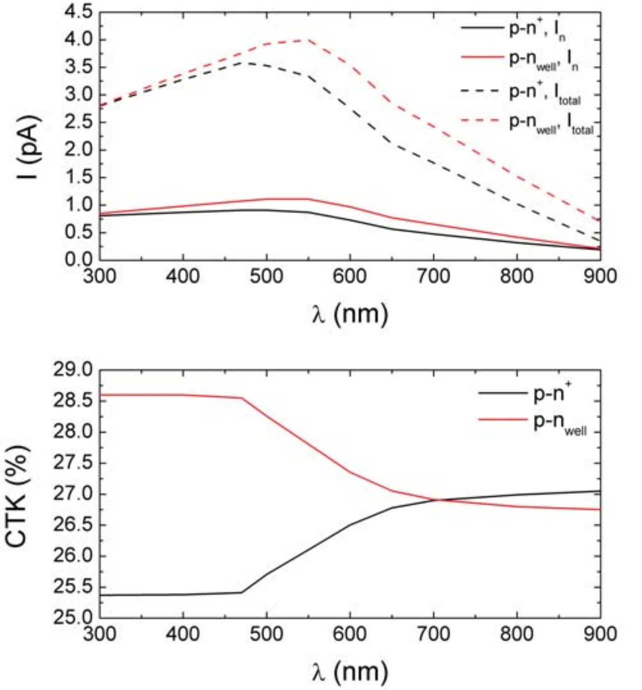


Fig. 8. p-n+ and p-nwell photodiodes comparison, both devices have the same diffusion and well areas, and also the same total width, $x_\ell = 5.06$ $\mu$m.

## VI. Conclusions

The continuous modeling activity of the last years with respect to photodiodes in the context of CMOS imager sensors has been reviewed in depth. We have written our revision accounting for semianalytical and analytical models; for the latter case, a one, two and three dimensional perspective has been employed to develop a coherent taxonomy of the models available in the literature. The pros and cons of the reviewed models have been presented within an articulate discussion taking into account a usual modeling trade-off between simplicity and accuracy. All the models presented have to be regarded, in their context, as steps forward to facilitate device engineering and circuit simulation of integrated circuits including CMOS imager sensors. Finally, some details of the latest achievements for the 2D modeling of the most common photodiode structures, accounting for the different current components and crosstalk effects, were given comparing with experimental and simulation data.

## References

[1] S. Morrison, "A new type of photosensitive junction device," *Solid State Electronics*, vol. 6, no. 5, pp. 485–494, 1963.

[2] J. Horton, R. Mazza, and D. H., "The scanistor - A solid-state image scanner," *Proceedings of the IEEE*, vol. 52, no. 12, pp. 1513–1528, 1964.

[3] M. Schuster and G. Strull, "A monolithic mosaic of photon sensors for solid-state imaging applications," *IEEE Transactions on Electron Devices*, vol. 13, no. 12, pp. 907–912, 1966.

[4] G. Weckler, "Operation of pn Junction Photodetectors in a Photon Flux Integrating Mode," *IEEE Journal of Solid-State Circuits.*, vol. 2, no. 3, pp. 65–73, 1967.

[5] P. Weimer, G. Sadasiv, J. Meyer Jr, L. Meray-Horvath, and W. Pike, "A self-scanned solid-state image sensor," *Proceedings of the IEEE*, vol. 55, no. 9, pp. 1591–1602, 1967.

[6] P. Noble, "Self-scanned silicon image detector arrays," *IEEE Trans. on Electron Devices,*, vol. 15, no. 4, pp. 202–209, 1968.

[7] R. Dyck and G. Weckler, "Integrated arrays of silicon photodetectors for image sensing," *IEEE Transactions on Electron Devices*, vol. 15, no. 4, pp. 196–201, 1968.

[8] S. Chamberlain, "Photosensitivity and scanning of silicon image detector arrays," *IEEE Journal of Solid-State Circuits*, vol. 4, no. 6, pp. 333–342, 1969.

[9] P. Fry, P. Noble, and R. Rycroft, "Fixed-pattern noise in photomatrices," *IEEE Journal of Solid-State Circuits*, vol. 5, no. 5, pp. 250–254, 1970.

[10] W. Boyle and S. G.E., "Charge coupled semiconductor devices," *Bell System Technical Journal*, vol. 49, no. 4, pp. 587–593, 1970.

[11] A. Theuwissen, *Solid-State Imaging With Charge-Coupled Devices*, ser. Solid-State Science and Technology Library. Springer, 1995.

[12] E. Fossum and D. Hondongwa, "A Review of the pinned photodiode for CCD and CMOS image sensors," *IEEE Journal of the Electron Devices Society*, vol. 2, no. 3, pp. 33–43, 2014.

[13] A. El Gamal, D. Yang, and B. Fowler, "Pixel Level Processing - Why, What, and How?" *Proc. SPIE*, vol. 3650, pp. 2–13, 1999.

[14] B. Fowler, A. El Gamal, and D. Yang, "A CMOS area image sensor with pixel-level A/D conversion," *1994 IEEE International Solid-State Circuits Conference, 1994. Digest of Technical Papers. 41st ISSCC.*, pp. 226–227, 1994.

[15] M. Snoeij, A. Theuwissen, K. Makinwa, and J. Huijsing, "Multiple-ramp column-parallel ADC architectures for CMOS image sensors," *IEEE Journal of Solid-State Circuits*, vol. 42, no. 12, pp. 2968–2977, 2007.

[16] M. Mori, M. Katsuno, S. Kasuga, T. Murata, T. Yamaguchi, M. Ind, and J. Kyoto, "A 1/4in 2M pixel CMOS image sensor with 1.75 transistor/pixel," *Digest of Technical Papers. IEEE International Solid-State Circuits Conference*, pp. 110–111, 2004.

[17] H. Wong, "Technology and device scaling considerations for CMOS imagers," *IEEE Trans. on Electron Devices*, vol. 43, no. 12, pp. 2131–2142, 1996.

[18] E. Fossum, "CMOS image sensors: electronic camera-on-a-chip," *IEEE Trans. on Electron Devices*, vol. 44, no. 10, pp. 1689–1698, 1997.

[19] A. El Gamal, "Trends in CMOS image sensor technology and design," *Digest International Electron Devices Meeting*, pp. 805–808, 2002.

[20] H. Rhodes, G. Agranov, C. Hong, U. Boettiger, R. Mauritzson, J. Ladd, I. Karasev, J. McKee, E. Jenkins, W. Quinlin *et al.*, "CMOS imager technology shrinks and image performance," *IEEE Workshop on Microelectronics and Electron Devices*, pp. 7–18, 2004.

[21] P. Catrysse and B. Wandell, "Roadmap for CMOS image sensors: Moore meets Planck and Sommerfeld," *Proc. SPIE.*, vol. 5678, pp. 1–13, 2005.

[22] A. Theuwissen, "CMOS image sensors: State-of-the-art," *Solid-State Electronics*, vol. 52, no. 9, pp. 1401–1406, 2008.

[23] J. Shappir and A. Kolodny, "The response of small photovoltaic detectors to uniform radiation," *IEEE Trans. on Electron Devices*, vol. 24, no. 8, pp. 1093–1098, 1977.

[24] H. Holloway, "Theory of lateral-collection photodiodes," *Journal of Applied Physics*, vol. 49, no. 7, pp. 4264–4269, 1978.

[25] H. Holloway and A. Brailsford, "Peripheral photoresponse of a p-n junction," *Journal of applied physics*, vol. 54, no. 8, pp. 4641–4656, 1983.

[26] D. Levy, S. Schacham, and I. Kidron, "Three dimensional analytical simulation of self- and cross-responsivities of photovoltaic detector arrays," *IEEE Trans. on Electron Devices*, vol. 34, pp. 2059–2069, 1987.

[27] I. Shcherback and O. Yadid-Pecht, "Photoresponse analysis and pixel shape optimization for CMOS active pixel sensors," *IEEE Trans. Electron Devices*, vol. 50, no. 1, pp. 12–18, 2003.

[28] ——, "Prediction of CMOS APS design enabling maximum photoresponse for scalable CMOS technologies," *IEEE Trans. on Electron Devices*, vol. 51, no. 2, pp. 285–288, 2004.

[29] I. Shcherback, T. Danov, and O. Yadid-Pecht, "A comprehensive CMOS APS crosstalk study: photoresponse model, technology, and design trends," *IEEE Trans. Electron Devices*, vol. 51, no. 12, pp. 2033–2041, 2004.

[30] B. Blanco-Filgueira, P. Lopez, D. Cabello, J. Ernst, H. Neubauer, and J. Hauer, "Bottom collection of photodiode-based CMOS APS," in *International Conference on Advanced Semiconductor Devices and Microsystems*, 2008, pp. 67–70.

[31] ——, "Sensitivity of photodiode-based CMOS APS in 0.18 $\mu$m technology: peripheral collection and optimum dimension," in *XXIII Conference on Design of Circuits and Integrated Systems*, 2008.

[32] ——, "Modeling and simulation of CMOS APS," in $7^{th}$ *Spanish Conference on Electron Devices*, 2009, pp. 120–123.

[33] B. Blanco-Filgueira, P. Lopez, D. Cabello, J. Hauer, and H. Neubauer, "Photoresponse model for photodiode-based CMOS APS in 180 nm and 90 nm technologies," in *XXV Conference on Design of Circuits and Integrated Systems*, 2010, pp. 37–45.

[34] T. Swe and K. Yeo, "An accurate photodiode model for DC and high frequency SPICE circuit simulation," in *Technical Proceedings of the International Conference on Modeling and Simulation of Microsystems*, vol. 1, no. 7, 2001, pp. 362–365.

[35] R. Perry and K. Arora, "Using PSPICE to simulate the photoresponse of ideal CMOS integrated circuit photodiodes," in *Proceedings of the IEEE Southeastcon.'Bringing Together Education, Science and Technology'.*, 1996, pp. 374–380.

[36] W. Liu, O. Chen, L. Dai, P. Weng, K. Huang, and F. Jih, "A CMOS photodiode model," in *IEEE International Workshop on Behavioral Modeling and Simulation*, 2001, pp. 10–12.

[37] L. Ravezzi *et al.*, "A versatile photodiode SPICE model for optical microsystem simulation," *Microelectronics Journal*, vol. 31, no. 4, pp. 277–282, 2000.

[38] A. Alexandra, F. Dadouche, and P. Garda, "Two dimensional model for lateral photodiode," in *International Conference on Design and Test of Integrated Systems in Nanoscale Technology*, 2006, pp. 294–298.

[39] T. Naeve, M. Hohenbild, and P. Seegebrecht, "A new analytical compact model for two-dimensional finger photodiodes," *Solid-State Electronics*, vol. 52, no. 2, pp. 299–304, 2008.

[40] J. Lee and R. Hornsey, "Photoresponse of photodiode arrays for solid-state image sensors," *Journal of Vacuum Science & Technology A: Vacuum, Surfaces, and Films*, vol. 18, no. 2, pp. 621–625, 2000.

[41] C. Lin, B. Mathur, and M. Chang, "Analytical charge collection and MTF model for photodiode-based CMOS imagers," *IEEE Trans. on Electron Devices*, vol. 49, no. 5, pp. 754–761, 2002.

[42] D. Grois, I. Shcherback, T. Danov, and O. Yadid-Pecht, "Theoretical approach to CMOS APS PSF and MTF modeling-evaluation," *IEEE Sensors Journal*, vol. 6, no. 1, pp. 118–124, 2006.

[43] J. Lee, R. Hornsey, and D. Renshaw, "Analysis of CMOS Photodiodes. II. Lateral photoresponse," *IEEE Trans. Electron Devices*, vol. 50, no. 5, pp. 1239–1245, 2003.

[44] ——, "Analysis of CMOS photodiodes-Part I: quantum efficiency," *IEEE Trans. Electron Devices*, vol. 50, no. 5, pp. 1233–1238, 2003.

[45] B. Blanco-Filgueira, P. López, and J. Roldán, "Analytical modelling of size effects on the lateral photoresponse of CMOS photodiodes," *Solid-State Electronics*, vol. 73, no. 0, pp. 15–20, 2012.

[46] V. Dhar and V. Gopal, "Optimum diode geometry in a two-dimensional photovoltaic array," *Optical Engineering*, vol. 39, no. 8, pp. 2022–2030, 2000.

[47] ——, "Infrared detector performance in an array area," *Optical Engineering*, vol. 40, no. 5, pp. 679–691, 2001.

[48] S. U. Ay, "Spectral response improvement of CMOS APS pixel through lateral collection," *Proc. IEEE International Symposium on Circuits and Systems*, p. 4, 2006.

[49] S. Ay, "Photodiode Peripheral Utilization Effect on CMOS APS Pixel Performance," *IEEE Trans. on Circuits and Systems I: Regular Papers.*, vol. 55, no. 6, pp. 1405–1411, 2008.

[50] B. Blanco-Filgueira, P. López, J. Doge, M. Suárez, and J. Roldán, "Evidence of the lateral collection significance in small CMOS photodiodes," in *IEEE International Symposium onCircuits and Systems (ISCAS)*, 2012, pp. 3098–3101.

[51] L. Debnath, *Linear partial differential equations for scientists and engineers*. Birkhauser, 2007.

[52] B. Blanco-Filgueira, P. López, J. Roldán, and J. Hauer, "Analytical Model for Crosstalk in p-nwell Photodiodes," *IEEE Trans. Electron Devices*, vol. 62, no. 2, pp. 580–586, 2015.

[53] B. Blanco-Filgueira, P. López, and J. B. Roldán, "Experimental characterization of peripheral photocurrent in CMOS photodiodes down to 65 nm technology," *Semicond. Sci. Technol.*, vol. 28, no. 4, pp. 045 011–045 017, 2013.

[54] F. Pêcheux, C. Lallement, and A. Vachoux, "VHDL-AMS and Verilog-AMS as alternative hardware description languages for efficient modeling of multidiscipline systems," *IEEE Transactions on Computer-Aided Design of Integrated Circuits and Systems*, vol. 24, no. 2, pp. 204–225, 2005.

[55] F. Mieyeville, M. Brière, I. O'Connor, F. Gaffiot, and G. Jacquemod, "A VHDL-AMS library of hierarchical optoelectronic device models," *Languages for system specification*, pp. 183–199, 2004.

[56] "Compact Verilog-A pn junction photodiode model," http://qucs.sourceforge.net/docs/photodiode.pdf.

[57] F. Dadouche, A. Alexandre, B. Granado, A. Pinna, and P. Garda, “A VHDL-AMS spectral model of photodetectors for active pixel sensors,” in *Forum on Specification and Design Languages*, 2002, pp. 24–27.

[58] F. Dadouche, A. Pinna, P. Garda, and A. Alexandre, “Modelling of pixel sensors for image systems with VHDL-AMS,” *Int. Journal of Electron.*, vol. 95: 3, pp. 211–225, 2008.

[59] G. Agranov, V. Berezin, and R. H. Tsai, “Crosstalk and microlens study in a color CMOS image sensor,” *IEEE Trans. Electron Devices*, vol. 50, no. 1, pp. 4–11, 2003.

[60] L. Blockstein and O. Yadid-Pecht, “Crosstalk quantification, analysis, and trends in CMOS image sensors,” *Applied optics*, vol. 49, no. 24, pp. 4483–4488, 2010.

[61] C. H. Tseng, S. G. Wuu, H. C. Chien, D. N. Yaung, T. H. Hsu, J. S. Lin, H. J. Hsu, C. Y. Yu, C. H. Lo, and C. S. Wang, “Crosstalk Improvement Technology Applicable to 0.14$\mu$m CMOS Image Sensor,” in *IEEE Int. Electron Devices Meeting Tech. Dig.*, 2004, pp. 997–1000.

[62] M. Estribeau and P. Magnan, “Pixel Crosstalk and Correlation with Modulation Transfer Function of CMOS Image Sensor,” in *Proc. SPIE*, vol. 5677, 2005, pp. 98–108.

[63] J. S. Lee, J. Shah, M. E. Jernigan, and R. I. Hornsey, “Characterization and Deblurring of Lateral Crosstalk in CMOS image sensors,” *IEEE Trans. Electron Devices*, vol. 50, no. 12, pp. 2361–2368, 2003.

[64] H. Mutoh, “3-D Optical and Electrical Simulation for CMOS Image Sensors,” *IEEE Trans. Electron Devices*, vol. 50, no. 1, pp. 19–25, 2003.

[65] F. Zhang, J. Zhang, C. Yang, and X. Zhang, “Performance Simulation and Architecture Optimization for CMOS Image Sensor Pixels Scaling Down to 1.0 $\mu$m,” *IEEE Trans. Electron Devices*, vol. 57, no. 4, pp. 788–794, 2010.

[66] I. Brouk, Y. Nemirovsky, S. Lachowicz, E. Gluszak, S. Hinckley, and E. K., “Characterization of crosstalk between CMOS photodiodes,” *Solid-State Electronics*, vol. 46, no. 1, pp. 53–59, 2002.

[67] I. Djite, M. Estribeau, P. Magnan, G. Rolland, S. Petit, and O. Saint-Pé, “Theoretical Models of Modulation Transfer Function, Quantum Efficiency, and Crosstalk for CCD and CMOS Image Sensors,” *IEEE Trans. Electron Devices*, vol. 59, no. 3, pp. 729–737, 2012.

[68] B. Blanco-Filgueira, P. López, and J. Roldán, “Closed-Form and explicit analytical model for crosstalk in CMOS photodiodes,” *IEEE Trans. Electron Devices*, vol. 60, no. 10, pp. 3459–3464, 2013.


**Beatriz Blanco-Filgueira** received the degree in physics and the Ph.D. degree from the University of Santiago de Compostela, Spain, in 2007 and 2012, respectively.

She is currently a postdoctoral researcher at CiTIUS and her research interests are the modeling of integrated circuits and semiconductor devices.

**Paula López Martínez** received the degree in physics and the Ph.D. degree from the University of Santiago de Compostela, Spain, in 1998 and 2003, respectively.

She is currently an Associate Professor at the University of Santiago de Compostela and author or coauthor of more than 50 research papers. Her current research interests include design of mixed signal integrated circuits and physical modeling of electronic devices.

**Juan Bautista Roldán Aranda** received the degree in physics and the Ph.D. degree from the University of Granada, Spain, in 1993 and 1997, respectively.

He is currently an Associate Professor at the University of Granada. His current research interests include modeling of nanometric conventional and multigate devices and Verilog-A implementation of device models for circuit simulation. He is the author or coauthor of more than 60 refereed technical journal papers and 70 communications at international conferences.